*J. Fluid Mech.* (1990), *vol.* 218, *pp.* 573–600
*Printed in Great Britain*



# A purely elastic instability in Taylor–Couette flow

By R. G. LARSON, ERIC S. G. SHAQFEH AND S. J. MULLER
AT&T Bell Laboratories, Murray Hill, NJ 07974, USA

(Received 6 July 1989)

A non-inertial (zero Taylor number) viscoelastic instability is discovered for Taylor–Couette flow of dilute polymer solutions. A linear stability analysis of the inertialess flow of an Oldroyd-B fluid (using both approximate Galerkin analysis and numerical solution of the relevant small-gap eigenvalue problem) show the growth of an overstable (oscillating) mode when the Deborah number exceeds $f(S)\,\epsilon^{-\frac{1}{2}}$, where $\epsilon$ is the ratio of the gap to the inner cylinder radius, and $f(S)$ is a function of the ratio of solvent to polymer contributions to the solution viscosity. Experiments with a solution of 1000 p.p.m. high-molecular-weight polyisobutylene in a viscous solvent show an onset of secondary toroidal cells when the Deborah number $De$ reaches 20, for $\epsilon$ of 0.14, and a Taylor number of $10^{-6}$, in excellent agreement with the theoretical value of 21. The critical $De$ was observed to increase as $\epsilon$ decreases, in agreement with the theory. At long times after onset of the instability, the cells become small in wavelength compared to those that occur in the inertial instability, again in agreement with our linear analysis. For this fluid, a similar instability occurs in cone-and-plate flow, as reported earlier. The driving force for these instabilities is the interaction between a velocity fluctuation and the first normal stress difference in the base state. Instabilities of the kind that we report here are likely to occur in many rotational shearing flows of viscoelastic fluids.

## 1. Introduction

In 1923, G. I. Taylor showed theoretically and experimentally that the simple circular shearing flow which occurs in a Couette cell at low rates of rotation of the inner cylinder (or low Reynolds numbers) becomes unstable as inertial forces are increased and is replaced by a flow with steady toroidal roll cells. This transition occurs at a critical value of the Taylor number, $T = [4\mu/(1+\mu)]Re^2(d/r_1)$, where $Re$ is the Reynolds number and $d$, $r_1$, and $\mu$ are the gap between the cylinders, the radius of the inner cylinder, and the ratio of the inner to outer cylinder radii, respectively. More recently, Coles (1965), Gollub & Swinney (1975), and others (Fenstermacher, Swinney & Gollub 1979) have documented the rich series of inertial transitions which occur in this Newtonian flow.

In the present study, we are concerned with the stability of a viscoelastic fluid in Taylor–Couette flow. In particular, we are interested in the possibility that, when inertia is absent, a secondary flow develops due solely to the viscoelastic character of the fluid. Thus our work is distinguished from that of most previous investigators, who considered the modifying effects of viscoelasticity on the inertial Taylor–Couette instability. Such experimental studies have been carried out by Rubin & Elata (1966), Denn & Roisman (1969), Sun & Denn (1972), Hayes & Hutton (1972), Jones, Davies & Thomas (1973), and others (Giesekus 1972; Beavers & Joseph 1974; Green & Jones 1982). In general, these workers found that viscoelasticity increases the

critical Taylor number at which a cellular flow is observed. Thus, the addition of viscoelasticity stabilizes the flow against the formation of inertial Taylor vortices. The wavenumber of the vortex cells at the critical Taylor number seems to be unaffected, however. Experiments by Giesekus (1972) are in agreement with these studies for dilute polymer solutions, but show an unexplained decrease in the critical Taylor number of up to 50% as the polymer concentration approaches 1000 p.p.m. In addition, Giesekus found that, for certain polymeric solutions, wave-like or oscillatory instabilities occur before stationary vortices are established. The only report of a presumably non-inertial transition is also from Giesekus (1966), who observed a Taylor-like cellular instability at $T = 10^{-2}$ for an uncharacterized polymeric solution.

Previous theoretical work (Datta 1964; Thomas & Walters 1964; Rubin & Elata 1966; Ginn & Denn 1969; Sun & Denn 1972) concerning the influence of viscoelasticity on Taylor–Couette flow has shown that for small gaps and weak viscoelasticity (to be defined below), the critical Taylor number is raised or lowered depending on the values of two dimensionless groups: $\Psi_1/2\rho d^2$ and $(\Psi_2/2\rho d^2)(r_1/d)$ (Ginn & Denn 1969). Here $\Psi_1 \equiv (\tau_{11}-\tau_{22})/\dot{\gamma}^2$ and $\Psi_2 \equiv (\tau_{22}-\tau_{33})/\dot{\gamma}^2$ are respectively the first and second normal stress coefficients in simple shearing flow and $\tau_{ii}$ is the normal stress in direction $i$ where '1' is the flow direction, '2' the gradient direction, and '3' the vorticity direction of the shearing flow. In addition, $\dot{\gamma}$ is the shear rate and $\rho$ is the fluid density. Positive values of both groups tend to destabilize the Taylor mode. Because the second group is proportional to $r_1/d$, it follows that for small enough gaps the role of $\Psi_2$ apparently becomes dominant, provided that $\Psi_2$ is not identically zero. Giesekus (1966) predicted theoretically that if $\Psi_2$ were positive and large in magnitude – i.e. $\Psi_2(\Psi_1+2\Psi_2)\dot{\gamma}^2/2\eta^2 > 1$, where $\eta$ is the shear viscosity – an instability would occur both in circular (Taylor) and plane Couette flow even with no inertia. For most polymeric solutions $\Psi_2$, however, is usually found to be small – much smaller than $\Psi_1$ – and negative in sign (Keentok *et al.* 1980). Thus Giesekus' zero-inertia instability is not expected to be observed. Furthermore, if $\Psi_2$ is negative then the inertial Taylor instability should be stabilized by viscoelasticity in the small-gap limit, which is consistent with most experiments (Rubin & Elata 1966; Denn & Roisman 1969; Jones *et al.* 1973).

The term 'weak viscoelasticity', as used in the above discussion, means that the rheological behaviour of the fluid in the regime of flow rates considered is that of a second-order fluid; i.e. the lowest order perturbation from a first-order or Newtonian fluid. For highly elastic fluids, the second-order equation is inadequate in describing the fluid rheology and one must specify a more complex constitutive relationship. Analyses of the Taylor–Couette instability have been carried out for several complex constitutive equations; the most general analyses are those of Lockett & Rivlin (1968), Smith & Rivlin (1972), and Miller & Goddard (1979) for the general viscoelastic 'simple fluid'. For a 'simple fluid', the stress in a fluid element is a continuous functional of the kinematic history of that element alone and not of neighbouring elements (Coleman & Noll 1961). Comparison of these theoretical results with experiments is hampered, however, by the large number of viscoelastic parameters contained in the models. For example, in Lockett & Rivlin's analysis of the 'simple' fluid, there are nine such parameters. Such a complex constitutive equation may be required for describing melts or concentrated solutions of flexible polymer molecules (which we note are strongly shear thinning and usually have values of $\Psi_2/\Psi_1$ in the range $-0.10$ to $-0.30$ (Keentok *et al.* 1980; Ramachandran, Gao & Christiansen 1985)). However, dilute polymer solutions (i.e. concentration less

than $\sim 0.1\,\%$) of flexible high-molecular-weight polymers seem to be reasonably well described by the simpler three-parameter Oldroyd-B equation, presented shortly. This equation predicts no shear thinning, and a constant first normal stress coefficient, which is consistent with measurements of dilute-solution properties (Boger 1977; Sridhar *et al.* 1986; Mackay & Boger 1987). The Oldroyd-B equation also predicts that the second normal stress difference is zero. This is in at least rough accord with recent measurements showing that $\Psi_2/\Psi_1$ is close to zero for these fluids (Keentok *et al.* 1980; Magda *et al.* 1990).

In 1967, Beard, Davies & Walters analysed the stability of Taylor–Couette flow with the upper-convected Maxwell equation, a special case of the Oldroyd-B equation. Viscoelastic effects, as described by this constitutive equation, destabilize Taylor's mode. In addition, when the Deborah number – which is the product of the typical shear rate and the characteristic relaxation time of the fluid – is increased above a threshold, the solution bifurcates, and a new mode of instability appears. This mode is overstable – i.e. it is time-periodic, and for highly elastic fluids it reduces the critical Taylor number by a factor of 100 below that required for the instability in Newtonian fluids.

To our knowledge, all the previous theoretical work on viscoelastic Taylor–Couette flow (for realistic values of the second normal stress coefficient) concerns those modifications of the inertial instability that are produced by viscoelasticity. In this paper we shall show that for the Oldroyd-B fluid there exists an inertia-free mode of instability in Taylor–Couette flow. The instability is time-periodic, is driven by a coupling of the first normal-stress difference in a curvilinear base shearing flow to velocity fluctuations, and seems to be closely related both to cone-and-plate and plate-and-plate instabilities predicted by Phan-Thien (1983, 1985). In addition, experiments performed with a fluid for which the Oldroyd-B equation is a good description, namely a dilute solution of a flexible high-molecular-weight polymer in a viscous solvent (a Boger fluid), show the existence of a non-inertial cellular instability. Measurements of the wavenumber characterizing the instability are in agreement with the theoretical predictions. The critical Deborah number $De_c$ and its dependence on the dimensionless gap thickness has also been measured and is in agreement with our theory.

## 2. Linear stability analysis

To describe the rheology of the fluid used in our experiments, we use the Oldroyd-B constitutive equation, for which the stress tensor $\boldsymbol{\tau}$ is given by the sum of two terms,

$$\boldsymbol{\tau} = \boldsymbol{\tau}^{\mathrm{p}} + \boldsymbol{\tau}^{\mathrm{s}}. \tag{2.1}$$

The first term can be considered the polymeric contribution, while the second is due to the Newtonian solvent:

$$\boldsymbol{\tau}^{\mathrm{s}} \equiv 2\eta_{\mathrm{s}} \boldsymbol{D}. \tag{2.2}$$

In (2.2), $\boldsymbol{D}$ is the rate-of-strain tensor, which is the symmetric part of the velocity gradient,

$$2\boldsymbol{D} \equiv \boldsymbol{\nabla v} + (\boldsymbol{\nabla v})^{\mathrm{T}}, \tag{2.3}$$

and $\eta_{\mathrm{s}}$ is the solvent viscosity. The polymeric contribution to the stress tensor satisfies the upper-convected Maxwell equation:

$$\lambda \overset{\nabla}{\boldsymbol{\tau}}^{\mathrm{p}} + \boldsymbol{\tau}^{\mathrm{p}} = 2\eta_{\mathrm{p}} \boldsymbol{D}, \tag{2.4}$$

where $\eta_p$ is the polymeric contribution to the shear viscosity and $\lambda$ is the polymer relaxation time. The $\overset{\nabla}{}$ above $\boldsymbol{\tau}^p$ denotes the upper-convected derivative defined as

$$\overset{\nabla}{\boldsymbol{S}} \equiv \frac{\partial}{\partial t}\boldsymbol{S} + \boldsymbol{v}\cdot\nabla\boldsymbol{S} - (\nabla\boldsymbol{v})^{\mathrm{T}}\cdot\boldsymbol{S} - \boldsymbol{S}\cdot\nabla\boldsymbol{v}. \tag{2.5}$$

The Oldroyd-B constitutive equation, which can be derived from a molecular model in which the polymer molecule is idealized as a Hookean spring connecting two Brownian beads (Bird *et al.* 1987), contains the Newtonian fluid ($\eta_p = 0$) and the upper-convected Maxwell fluid ($\eta_s = 0$) as special cases. The first normal stress coefficient, $\Psi_1$, equals $2\eta_p\lambda$.

In the present development we shall only consider axisymmetric flows, and thus Cauchy's equations of motion become

$$\rho\left(\frac{\partial v_r}{\partial t} + v_r\frac{\partial v_r}{\partial r} - \frac{v_\theta^2}{r} + v_z\frac{\partial v_r}{\partial z}\right) = \left[\frac{1}{r}\frac{\partial}{\partial r}(r\tau_{rr}) - \frac{\tau_{\theta\theta}}{r} + \frac{\partial}{\partial z}\tau_{zr}\right] - \frac{\partial p}{\partial r}, \tag{2.6}$$

$$\rho\left(\frac{\partial v_\theta}{\partial t} + v_r\frac{\partial v_\theta}{\partial r} + \frac{v_r v_\theta}{r} + v_z\frac{\partial v_\theta}{\partial z}\right) = \left[\frac{1}{r^2}\frac{\partial}{\partial r}(r^2\tau_{r\theta}) + \frac{\partial}{\partial z}\tau_{z\theta}\right], \tag{2.7}$$

$$\rho\left(\frac{\partial v_z}{\partial t} + v_r\frac{\partial v_z}{\partial r} + v_z\frac{\partial v_z}{\partial z}\right) = \left[\frac{1}{r}\frac{\partial}{\partial r}(r\tau_{rz}) + \frac{\partial}{\partial z}\tau_{zz}\right] - \frac{\partial p}{\partial z}, \tag{2.8}$$

where $\rho$ is the fluid density. The equation of continuity for the axisymmetric flow of an incompressible fluid is

$$\frac{1}{r}\frac{\partial}{\partial r}(rv_r) + \frac{\partial}{\partial z}v_z = 0. \tag{2.9}$$

Finally, for the cylindrical Couette geometry the no-slip and no-penetration boundary conditions are

$$\left.\begin{aligned} &v_r = v_z = 0 \quad \text{at} \quad r = r_1, r_2 \\ &v_\theta = r_1\Omega_1 \quad \text{at} \quad r = r_1; \quad v_\theta = r_2\Omega_2 \quad \text{at} \quad r = r_2, \end{aligned}\right\} \tag{2.10}$$

where $\Omega_1$ and $\Omega_2$ are the rotation rates of the inner and outer cylinder, respectively.

For the constitutive equation that we have chosen, the above equations are all satisfied by the simple shearing flow,

$$v_r^0 = v_z^0 = 0; \quad v_\theta^0 \equiv V^0 = Ar + Br^{-1}, \tag{2.11a}$$

with

$$A \equiv \frac{r_2^2\Omega_2 - r_1^2\Omega_1}{r_2^2 - r_1^2}; \quad B \equiv \frac{r_1^2 r_2^2(\Omega_1 - \Omega_2)}{r_2^2 - r_1^2}. \tag{2.11b}$$

The superscript 0 is used to denote the base flow. In addition, the components of the stress contribution $\boldsymbol{\tau}^p$ are

$$\tau_{rr}^0 = \tau_{zz}^0 = \tau_{rz}^0 = \tau_{\theta z}^0 = 0; \quad \tau_{r\theta}^0 = -2\eta_p Br^{-2}; \quad \tau_{\theta\theta}^0 = 8\eta_p\lambda B^2 r^{-4}, \tag{2.12}$$

where the superscript p has been dropped.

We now consider the evolution of a small normal-mode perturbation added to the

base solution. For axisymmetric disturbances, the velocities and polymeric stresses become

$$v_r = U(r)\,e^{i(\sigma z-\omega t)}; \quad v_\theta = v_\theta^0 + V(r)\,e^{i(\sigma z-\omega t)}; \quad v_z = W(r)\,e^{i(\sigma z-\omega t)}, \tag{2.13a}$$

$$p = p^0 + p(r)\,e^{i(\sigma z-\omega t)}, \tag{2.13b}$$

$$\left.\begin{aligned}(\tau_{rr})^p &= \widehat{RR}(r)\,e^{i(\sigma z-\omega t)}; \quad (\tau_{r\theta})^p = \tau_{r\theta}^0 + \widehat{R\Theta}(r)\,e^{i(\sigma z-\omega t)}; \quad (\tau_{\theta\theta})^p = \tau_{\theta\theta}^0 + \widehat{\Theta\Theta}(r)\,e^{i(\sigma z-\omega t)};\\ (\tau_{rz})^p &= \widehat{RZ}(r)\,e^{i(\sigma z-\omega t)}; \quad (\tau_{\theta z})^p = \widehat{\Theta Z}(r)e^{i(\sigma z-\omega t)}; \quad (\tau_{zz})^p = \widehat{ZZ}(r)\,e^{i(\sigma z-\omega t)}.\end{aligned}\right\} \tag{2.13c}$$

We shall be considering the temporal stability of the flow, so $\omega$ is in general a complex frequency and $\sigma$ is the real wavenumber. This formulation allows for the consideration of overstable as well as stationary modes.

In Appendix A it is shown that when the expressions (2.11)–(2.13) are substituted into the continuity equation (2.9), the momentum balance equations (2.6)–(2.8), and the constitutive equations (2.1)–(2.5), and the resulting system of equations is linearized in the disturbances, in the 'small-gap' limit one obtains (see (A 18)–(A 19)):

$$U'''' - 2\alpha^2 U'' + \alpha^4 U + De^2\,\epsilon\alpha^2\tilde{c}U' = 0 \tag{2.14}$$

with

$$\tilde{c} \equiv 2\left[\frac{D^{-2}(1+2D^{-1})(D^{-1}+S) - D^{-3}(1+D^{-1})}{(D^{-1}+S)^2}\right], \tag{2.15}$$

where

$$D \equiv 1 - i\hat{\omega}. \tag{2.16}$$

In the derivation of (2.14)–(2.16), we have neglected inertial effects (defining $Re \equiv \Omega_1 r_1 d\rho/(\eta_p+\eta_s) = 0$), and have taken $\epsilon \equiv d/r_1 \ll 1$. The primes in (2.14) denote differentiation with respect to the gap variable $x \equiv (r-r_1)/r_1$. In (2.14)–(2.16), the following dimensionless groups appear:

$$\left.\begin{aligned}&\epsilon \equiv \frac{d}{r_1}; \quad \alpha \equiv \sigma d,\\ &De \equiv \frac{(\Omega_1-\Omega_2)\lambda}{\epsilon}; \quad S \equiv \frac{\eta_s}{\eta_p}; \quad \hat{\omega} \equiv \omega\lambda.\end{aligned}\right\} \tag{2.17}$$

The boundary conditions for (2.14) are

$$U = U' = 0; \quad x = 0, 1. \tag{2.18}$$

As defined here, the Deborah number $De$ can be positive or negative, depending on the relative rotation rates and rotation directions of the inner and outer cylinders. Equation (2.14) along with (2.18) is an eigenvalue problem for $\hat{\omega}$, the solution of which we consider in the next section.

## 3. Solution of the eigenvalue problem

The eigenvalue problem for (2.14) can be written in the compact form

$$U'''' - 2\alpha^2 U'' + \alpha^4 U + \alpha^3 \Lambda U' = 0, \tag{3.1}$$

together with the boundary conditions, (2.18). In writing (3.1), we have defined $\Lambda = \epsilon De^2\tilde{c}/\alpha$ as the eigenvalue. We wish to find all possible eigensolutions of (3.1) and (2.18) and then calculate $\hat{\omega}$ using (2.15) and (2.16) to determine if the flow is unstable. Equation (3.1) together with (2.18) is a generalized eigenvalue problem that is not of Sturm–Liouville type. Thus previous literature gives little guidance as to the

existence and number of eigensolutions, or to a preferred solution technique. Therefore, we have used three different solution techniques, both to ensure the validity and accuracy of the solutions that we have found and to ensure that we have found the complete set of solutions.

### 3.1. *Approximate solution using Galerkin's method*

The simplest technique used is an approximate Galerkin method that relies on diagonal dominance of the inner-product matrices. This method has been applied to other stability problems (Drazin & Reid 1981), most notably to the Newtonian version of the Taylour–Couette problem by Chandrasekhar (1961), where the method proved remarkably successful. The application of the method to our problem is described in detail in Appendix B. The method leads to a simple calculation showing the existence of an infinite series of purely imaginary, conjugate eigenvalues. We shall show below that these solutions imply flow instability. To assess the accuracy of this approximate method, we also used two numerical solution methods that can be systematically refined to achieve any desired accuracy.

### 3.2. *Numerical solution methods*

#### 3.2.1. *Orthogonal shooting procedure*

The results obtained from the Galerkin method were confirmed and refined by calculations using two accurate numerical solution methods. The first is an orthogonal shooting procedure that two of the authors have used in a prvious study of the viscoelastic instability of falling film flow (Shaqfeh, Larson & Fredrickson 1989) and the instability in the inclined settling of small particles (Shaqfeh & Acrivos 1987). In the latter the method, based on the original ideas of Conte (1966), is described in detail. In short, two linearly independent initial solutions satisfying the boundary conditions at $x = 0$ are integrated across the gap according to (3.1). If we define the vector $\boldsymbol{U} = (U''', U'', U', U)$ then the initial conditions that we choose are

$$\boldsymbol{U}^1 = (1,0,0,0), \quad \boldsymbol{U}^2 = (0,1,0,0).$$

At each step in the integration we check the vector inner product between these two solutions to determine if, through the integration procedure, they are becoming linearly dependent. If they are (according to some predetermined criteria discussed in Shaqfeh *et al.* 1989) then the solutions are made orthonormal using the Gram–Schmidt procedure (Greenberg 1978). Note that in the present application, it was found that the eigenvalue problem is fairly stiff and that at least two orthonormalizations are required during integration to retain sufficient numerical accuracy in the solutions. This number increases as the wavenumber of the eigenmode increases. After each orthonormalization, the integration procedure is continued and the eigenvalue condition corresponding to the boundary conditions at $x = 1$ is applied, viz.

$$U^1U^{2\prime} - U^2U^{1\prime} = 0. \tag{3.2}$$

If the guessed eigenvalue does not satisfy this condition, the procedure is repeated until (3.2) is satisfied (again according to the criteria discussed in Shaqfeh *et al.* 1989). A complex secant method is used to obtain convergence on the eigenvalue. We use the results of the approximate Galerkin solution as initial eigenvalue guesses for this numerical procedure.

A comparison between the first three eigenvalues ($n = 1, 2, 3$) from the Galerkin method, (B 10), and the numerical results for a range of wavenumbers is found in table 1. For the dominant mode $n = 1$, the comparison is favourable, especially for

| | $\lvert\Lambda_n\rvert$, Approx. Galerkin | | | $\lvert\Lambda_n\rvert$, Orthog. shooting | | |
|---|---|---|---|---|---|---|
| $\alpha$ | $n=1$ | 2 | 3 | 1 | 2 | 3 |
| 1.0 | 429.32 | 3201.59 | — | 409.17 | 2550.5 | — |
| 2.0 | 60.48 | 413.85 | — | 57.30 | 329.47 | — |
| 3.0 | 21.89 | 129.57 | — | 20.50 | 103.22 | — |
| 4.0 | 12.09 | 58.95 | 179.67 | 11.10 | 47.14 | 133.71 |
| 5.0 | 8.48 | 33.17 | 96.23 | 7.57 | 26.72 | 71.81 |
| 6.0 | 6.89 | 21.45 | 58.77 | 5.92 | 17.47 | 44.01 |
| 7.0 | 6.12 | 15.31 | 39.39 | 5.03 | 12.64 | 29.77 |
| 8.0 | 5.76 | 11.77 | 28.30 | 4.50 | 9.84 | 21.59 |

TABLE 1. Comparison of eigenvalue calculations

small wavenumbers. Near the critical value ($\alpha_c = 6.7$) the Galerkin result is too high by 16%. Various error checks – including grid refinement, convergence tests etc. – were applied to the numerical results presented in table 1 and the results tabulated are accurate to at least the first four decimal places. We thus conclude that the Galerkin method gives a good approximation for the infinite series of eigenvalues $\Lambda_n$.

3.2.2. *Direct method*

Because of our concern that we uncover all modes of the linear stability problem posed by (2.14)–(2.18), another method, the direct method, was used to solve the eigenvalue problem. To describe the direct method, we note that since (2.14) has coefficients that are independent of $x$, the eigenfunctions are simple exponentials:

$$U = \exp(\lambda_i x); \quad i = 1, 2, 3, 4. \tag{3.3}$$

The $\lambda_i$ are the roots of the characteristic equation

$$(\lambda_i^2 - \alpha^2)^2 + \alpha^3 \Lambda \lambda_i = 0. \tag{3.4}$$

These roots were found using the general formulae for solutions to quartic polynomials. Only the case of non-degenerate roots was considered in our application of the direct method. The possibility of degenerate roots is allowed in the shooting method described above, but no such roots were ever found to be solutions of the full eigenvalue problem with the boundary conditions. A solution to (3.4) for non-degenerate roots must be

$$U = \sum_{i=1}^{4} A_i \exp(\lambda_i x). \tag{3.5}$$

Four boundary conditions – namely, $U = U' = 0$ at $x = 0, 1$ – must be satisfied. The boundary conditions at $x = 0$ imply that

$$\sum_{i=1}^{4} A_i = 0; \quad \sum_{i=1}^{4} \lambda_i A_i = 0, \tag{3.6a}$$

while those at $x = 1$ imply

$$\sum_{i=1}^{4} A_i \exp(\lambda_i) = 0; \quad \sum_{i=1}^{4} \lambda_i A_i \exp(\lambda_i) = 0. \tag{3.6b}$$

Since these boundary conditions are homogeneous, the system will have a non-zero solution only if the following determinant condition is satisfied:

$$\det\begin{pmatrix} 1 & 1 & 1 & 1 \\ \lambda_1 & \lambda_2 & \lambda_3 & \lambda_4 \\ e^{\lambda_1} & e^{\lambda_2} & e^{\lambda_3} & e^{\lambda_4} \\ \lambda_1 e^{\lambda_1} & \lambda_2 e^{\lambda_2} & \lambda_3 e^{\lambda_3} & \lambda_4 e^{\lambda_4} \end{pmatrix} = 0. \tag{3.7}$$

The eigenvalues are then determined by starting with an initial guess, finding the four roots $\lambda_i$ of (3.4), calculating the determinant in (3.7), and finally iterating on the initial eigenvalue guess using the secant method until the determinant is made vanishingly small. Values of $\Lambda$ obtained this way were always the same as those found by the orthogonal shooting method. We also calculated both the real and imaginary parts of the determinant of (3.7) for a large region of the complex-$\Lambda$ plane. The eigenvalues determined by the orthogonal shooting procedure described above were verified and no other solutions in the complex plane were uncovered. Thus, in the discussion and figures that follow all numerical solutions are those calculated by the orthonormal shooting procedure.

## 4. Stability results

### 4.1. *The Maxwell fluid*; $S = 0$

With the eigenvalue solutions for $\Lambda_n$, it is only a matter of algebra to relate the complex frequency, $\hat{\omega}$, to the $\Lambda_n$ through the expression for $\tilde{c}$ in (2.15) above. We first discuss this relation in terms of the Maxwell fluid, $S = 0$. In this instance, algebraic manipulations of (2.15) yield the following two relations between the real and imaginary parts of $\hat{\omega}$ and $\Lambda_n$:

$$\mathrm{Im}\,(\Lambda_n) = \frac{2\epsilon De^2}{\alpha}\frac{2\hat{\omega}_r(\hat{\omega}_i+1)}{[(\hat{\omega}_i+1)^2+\hat{\omega}_r^2]^2}, \tag{4.1a}$$

$$\mathrm{Re}\,(\Lambda_n) = \frac{2\epsilon De^2}{\alpha}\frac{(\hat{\omega}_i+1)^2-\hat{\omega}_r^2}{[(\hat{\omega}_i+1)^2+\hat{\omega}_r^2]^2}, \tag{4.1b}$$

where $\hat{\omega}_r$ and $\hat{\omega}_i$ are the real and imaginary parts of the complex frequency respectively. Since the eigenvalues $\Lambda_n$ calculated by the procedures described previously are all purely imaginary, it follows that the solution of (4.1) is

$$\hat{\omega}_r = \pm(\hat{\omega}_i+1), \tag{4.2a}$$

$$(\hat{\omega}_i+1)^2 = \frac{\epsilon De^2}{\alpha|\Lambda_n|}, \tag{4.2b}$$

where $|\Lambda_n|$ is the magnitude of the imaginary eigenvalue $\Lambda_n$. Because the flow is unstable if $\hat{\omega}_i > 0$ and because the absolute magnitude of $\Lambda_n$ increases with increasing $n$, (4.2$b$) defines a critical condition for instability as

$$\frac{\epsilon De^2}{\alpha|\Lambda_1(\alpha)|} \geqslant 1. \tag{4.3}$$

According to (4.2$b$), for sufficiently large values of the Deborah number each successive mode will be unstable. From (4.2$a$) all these modes are overstable and for the Maxwell fluid, they propagate or oscillate at the neutral point with exactly the

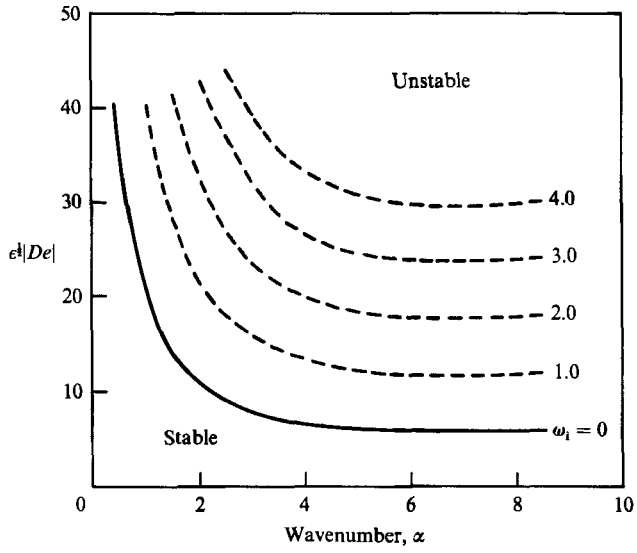


FIGURE 1. Curves of constant growth rate of the most unstable mode for the Maxwell fluid, calculated from (4.2*b*) with the orthogonal shooting procedure.

characteristic relaxation time of the polymeric fluid. (Note the Oldroyd-B equation assumes a single relaxation time and this time can be thought of as some average relaxation time of the real fluid.) From the numerical solutions presented previously, we find that $\alpha|\Lambda_1(\alpha)|$ is a minimum at $\alpha = 6.7 \pm 0.1$ and so the precise critical condition for the Maxwell fluid becomes

$$\alpha_c = 6.7 \pm 0.1, \quad [\epsilon^{\frac{1}{2}}|De|]_c = 5.92 \pm 0.02. \tag{4.4}$$

In figure 1, we have plotted the neutral curve that corresponds to the relation

$$\epsilon^{\frac{1}{2}}|De| = [\alpha|\Lambda_1|]^{\frac{1}{2}}, \tag{4.5}$$

along with a number of curves of constant wave growth that are determined from (4.2*b*). Note that the minimum in the neutral curve (corresponding to the critical condition delineated above) is a shallow one, suggesting that small changes about the critical condition may cause a spectrum of wavelengths to become unstable. It can be shown, however, that the value of $\epsilon^{\frac{1}{2}}|De|$ necessary for instability uniformly increases for values of $\alpha$ in excess of 6.7. In fact an asymptotic analysis shows that the $\Lambda_n$ are all $O(1)$ in the limit $\alpha \to \infty$, and they are the solutions of the following eigenvalue problem:

$$U'''' - 2U'' + U + \Lambda U' = 0, \tag{4.6a}$$

with the boundary conditions

$$U = U' = 0; \quad x = 0, \infty. \tag{4.6b}$$

The eigenvalue with the smallest absolute value for this problem was found numerically to be $\Lambda_1 = \pm i3.84$. Thus, from (4.3) the limiting form for the neutral curve pictured in figure 1 for large $\alpha$ is

$$[\epsilon^{\frac{1}{2}}|De|] \to 1.960 \ldots \alpha^{\frac{1}{2}}, \quad \alpha \to \infty. \tag{4.7}$$

Numerical solutions of the eigenvalue problem for finite values of $\alpha$ show that deviations from this asymptote remain significant (greater than 1%) until $\alpha$ is as large as 20 or more.

### 4.2. *The Oldroyd-B fluid*; $S > 0$

Although our analysis of the Maxwell fluid is a useful starting point, all the fluids that can be realized in the laboratory and are rheologically described by the Oldroyd-B equation have values of $S$ in excess of unity. To describe the stability of the Taylor–Couette flows of these fluids, we need only modify the discussion that we have previously presented. In this analysis, however, the algebra is more complicated and we shall therefore limit our discussion of analytic results to the modifications of the neutral curves.

Returning to (2.15) and setting $\hat{\omega}_i = 0$, we can use the relation between $\tilde{c}$ and $\Lambda$ to obtain two expressions that are the analogues of (4.1) for arbitrary $S$. The first expression is derived from the fact that the real part of $\Lambda_n$ is always zero and gives the value of $\hat{\omega}_r$ in terms of the only real root of the cubic equation

$$S^3\chi^3+S(7S^2+S-1)\chi^2+(3S^3+2S^2+2S+1)\chi-(3S^3+7S^2+5S+1)=0, \quad (4.8)$$

with $\chi = \hat{\omega}_r^2$. The second expression then gives the critical condition and the equation for the neutral curve which is the analogue of (4.5), viz.

$$\frac{\epsilon De^2 K(S)}{\alpha|\Lambda_1(\alpha)|} \geqslant 1, \quad (4.9a)$$

where $K(S)$ is given by the expression

$$K = \frac{4\chi^{\frac{1}{2}}[S\chi^2+4S^2(S+1)\chi+(4S^3+7S^2+4S+1)]}{[1+\chi]^2[(S+1)^2+\chi S^2]^2}. \quad (4.9b)$$

With these results, we can now draw some general conclusions concerning the change in the neutral conditions for non-zero values of $S$. First, one can solve numerically for $\chi$ and show that for $0 \leqslant S \leqslant 1$, $\chi$ and $K(S)$ differ from unity by only a few percent. In fact, for $S = 1$, $\chi$ and $K$ are identically equal to 1 as a consequence of the fact that $\tilde{c}(0) = \tilde{c}(1)$ (to verify this cf (2.15)). Thus it follows that the flow stability is not affected significantly until $S$ is increased from unity, which, as we have previously mentioned, is also the parameter regime of experimental interest.

For values of $S \geqslant \alpha$, $\chi(S)$ is monotonically decreasing from $\chi = 1$ at $S = 1$ to $\chi \to 0.475\ldots$ as $S \to \infty$. Thus, the oscillation frequency ($\hat{\omega}_r = \pm\chi^{\frac{1}{2}}$) of the overstable mode near the neutral point decreases to approximately 70% of the polymer relaxation frequency (i.e. $1/\lambda$) as $S$ is increased. In addition, $K(S)$ monotonically decreases as $S$ is increased beyond unity, and for large $S$, $K \to 3.436\ldots/S$. From (4.9$a$), this shows that the critical Deborah number increases as the solvent viscosity is increased. Or, in other words, viscous effects are stabilizing, which is the result one would expect intuitively. The neutral curve, for non-zero values of $S$, is now defined by the relation

$$\epsilon^{\frac{1}{2}}|De| = \left[\frac{\alpha|\Lambda_1|}{K(S)}\right]^{\frac{1}{2}} \quad (4.10a)$$

and the critical condition defined by (4.4) for the Maxwell fluid is now modified to

$$\alpha_{\text{crit}} = 6.7 \pm 0.1, \quad [\epsilon^{\frac{1}{2}}|De|]_{\text{crit}} = \frac{5.92 \pm 0.02}{K^{\frac{1}{2}}}. \quad (4.10b)$$

We have plotted the modified neutral curves for various values of $S$ in figure 2 showing the stabilizing effect of viscous forces. All the curves show the same

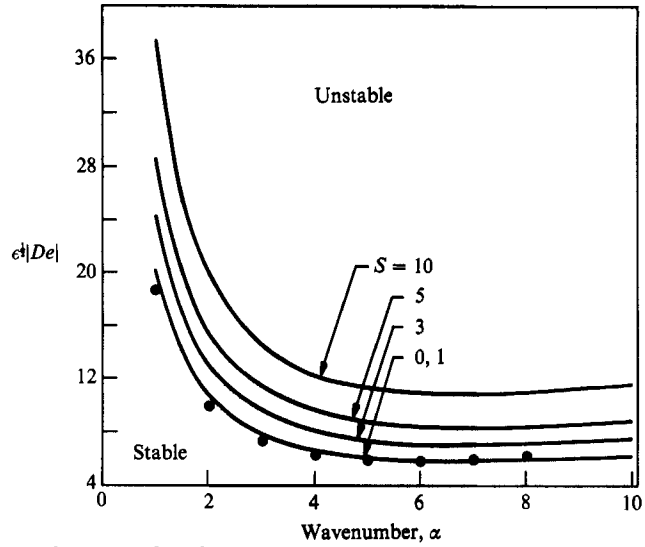


FIGURE 2. Neutral curves for the most unstable mode calculated by the orthogonal shooting procedure (lines) for various values of $S$. Also shown are the calculations using the approximate Galerkin technique (points) for $S = 0$.

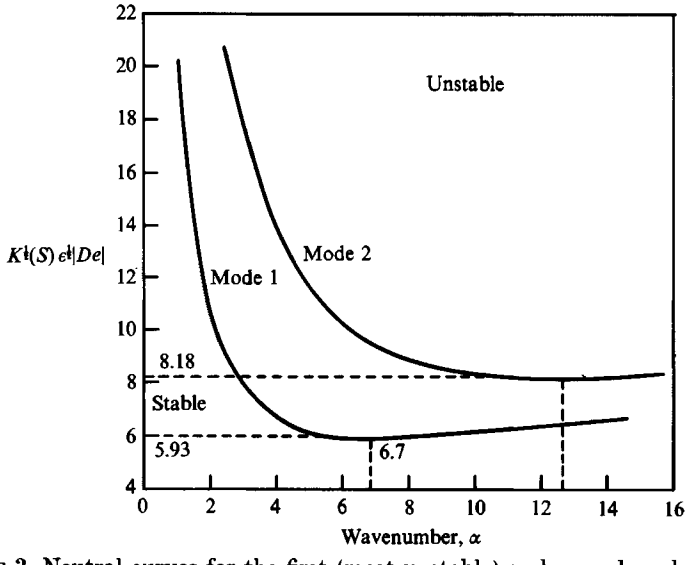


FIGURE 3. Neutral curves for the first (most unstable) and second mode of the instability.

relatively shallow minimum although as $S$ is increased the 'well' becomes slightly steeper. Note that for large values of the wavenumber our aforementioned asymptotic analysis can be modified to show that the neutral curves approach the limit

$$\epsilon^{\frac{1}{3}}|De| \to \frac{1.960\ldots}{K^{\frac{1}{3}}}\alpha^{\frac{1}{3}}; \quad \alpha \to \infty. \tag{4.11}$$

Thus, a slightly steeper rise in $\epsilon^{\frac{1}{3}}|De|$ is predicted. In figure 3, we have plotted the neutral curves ($K^{\frac{1}{3}}(S)\,\epsilon^{\frac{1}{3}}|De|$ *vs.* $\alpha$) for the first two modes of the viscoelastic instability. This latter plot shows that the critical Deborah number for the second mode is significantly larger (by a factor of 1.38) than that for the most unstable mode.

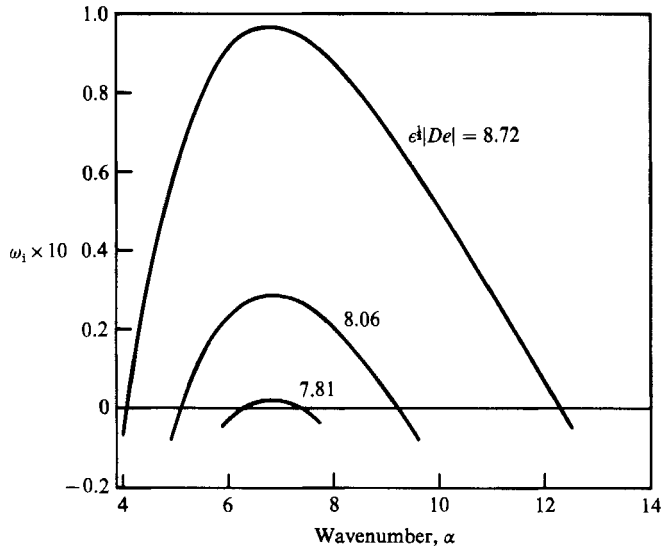


FIGURE 4. The growth factor, $\omega_i \times 10$ of the most unstable mode at various values of $\epsilon^{\frac{1}{2}}|De|$ for $S = 4$. $\epsilon^{\frac{1}{2}}|De|_c = 7.77$.

Finally to conclude this section, we have calculated numerically several growth rates of the most unstable mode for $S = 4$ and several values of $\epsilon^{\frac{1}{2}}|De|$. These are plotted in figure 4. Our numerical calculations show that the growth rates are monotonically increasing functions of $\epsilon^{\frac{1}{2}}|De|$ and that the most unstable wavenumber changes only slightly as we move away from the neutral curve. Also, we note that clearly a broad band of wavelengths becomes unstable for small increases in $\epsilon^{\frac{1}{2}}|De|$ above the critical condition (cf. figure 4).

## 5. Experimental

### 5.1. *Viscoelastic fluid preparation and characterization*

The viscoelastic fluid used in this study was a polyisobutylene/polybutene 'Boger Fluid'. The high-molecular-weight species was a polyisobutylene obtained from Aldrich with a weight average molecular weight of 4 to 6 million and a broad molecular weight distribution. It was dissolved in trichloroethylene and then this solution was added to a low-molecular-weight polybutene (Parapol 950, from Exxon Chemicals; $M_w = 950$). The trichloroethylene was removed by heating the solution in a vacuum oven at 50 °C for four to six weeks. The final concentration of polyisobutylene in solution was 1000 p.p.m.

The test fluid was characterized in steady-shear and small-amplitude oscillatory flow between a cone and plate on the Rheometrics System IV rheometer. The temperature was $21.5 \pm 0.5$ °C. The steady-shear viscosity and primary normal-stress coefficient measurements are presented in figure 5. The steady shear material functions show Oldroyd-B behaviour for shear rates at least as high as 6.0 $s^{-1}$. Interpreting the data in terms of the Oldroyd-B model gives $\eta = \eta_p + \eta_s = 228$ P and $\Psi_1 = 2\lambda\eta_p = 750$ dyne $s^2/cm^2$ where we recall that the subscripts p and s refer to the polymeric and solvent contributions, respectively. The polybutene solvent has a viscosity that is constant at 180 P for shear rates up to 30 $s^{-1}$; this allows us to estimate $\eta_p \approx 48$ P and $\lambda \approx 7.8$ s.

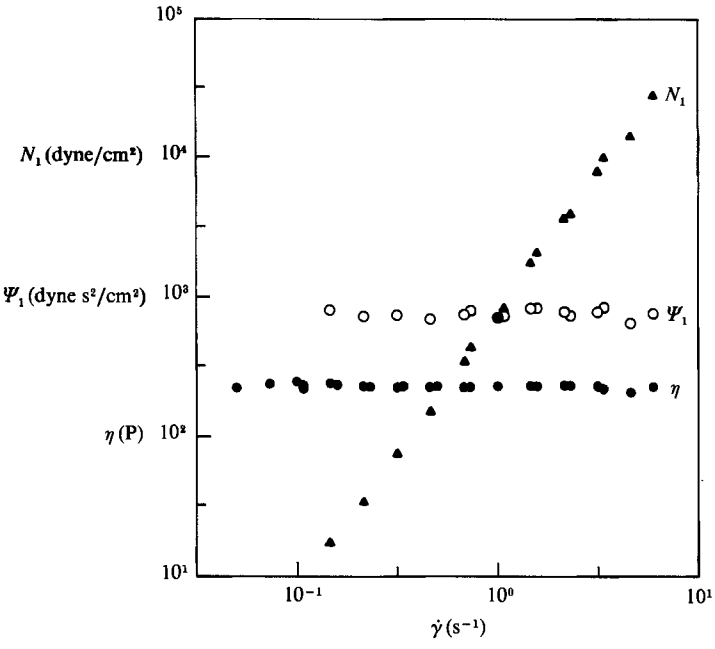


FIGURE 5. Viscosity $\eta$, first normal-stress difference $N_1$, and first normal-stress coefficient $\Psi_1$, as functions of shear rate for a high-molecular-weight Boger fluid.

The dynamic viscosity $\eta'$ in small-amplitude oscillatory shearing is shown as a function of frequency in figure 6. The storage modulus $G'$ (and hence $\eta''$) was too small to be resolved by the System IV. Since, for an Oldroyd-B fluid

$$\eta' = \frac{\eta_p}{1+\lambda^2\omega^2} + \eta_s, \tag{5.1}$$

one can also obtain estimates for $\eta_s$ and $\eta_p$ from these data. The values obtained in this way are in good agreement with those obtained from the steady-shear measurements. Also plotted in figure 6 is the dynamic viscosity for an Oldroyd-B fluid given by the above expression. The experimental values for $\eta'$ decrease more gradually with $\omega$ than predicted; this is indicative of a broad spectrum of relaxation times in the polydisperse test fluid.

Thus, the estimate $\lambda \approx 7.8$ s obtained from steady-state normal stress data is an average relaxation time. Other estimates of the relaxation time can be obtained by fitting the Oldroyd-B model to other measurements. Since alternate measurements weight the various relaxation times in the spectrum differently, a different average value of $\lambda$ may thereby be measured. Magda & Larson (1988), for example, found that fits of the Oldroyd-B model to measurements of transient shear-strain recovery and normal-stress relaxation gave relaxation times that were approximately twice as large as those obtained from measurements of steady-state normal stress. For the fluid studied here, a fit of the Oldroyd-B model to relaxation of normal stress also gives a value of $\lambda$, namely 16 s, that is about twice the value found from the steady-state normal stress; see figure 7. It is not clear *a priori* which average relaxation time should be chosen for comparison of theory to experiment in more complex flows, and in what follows we shall make comparisons using both of the above values.

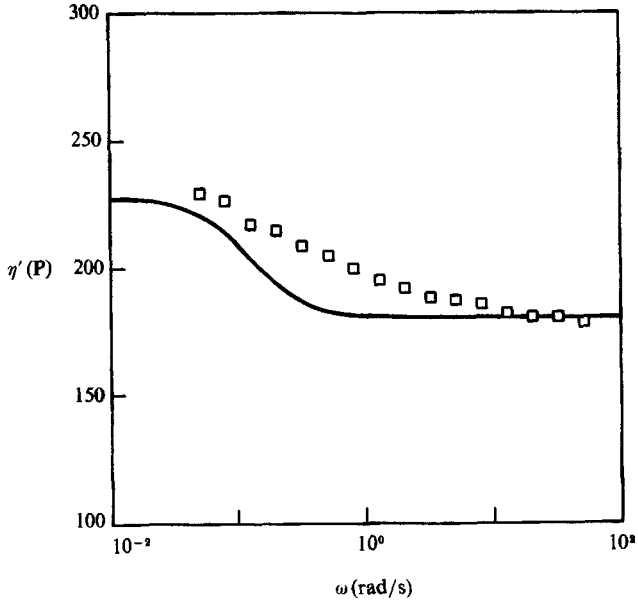


FIGURE 6. Dynamic viscosity $\eta'$ as a function of frequency $\omega$ in small-amplitude oscillatory shearing for a Boger fluid (symbols). The line is the prediction of the Oldroyd-B model where $\eta_s$, $\eta_p$, and $\lambda$ have been obtained by fits to steady-shear data.

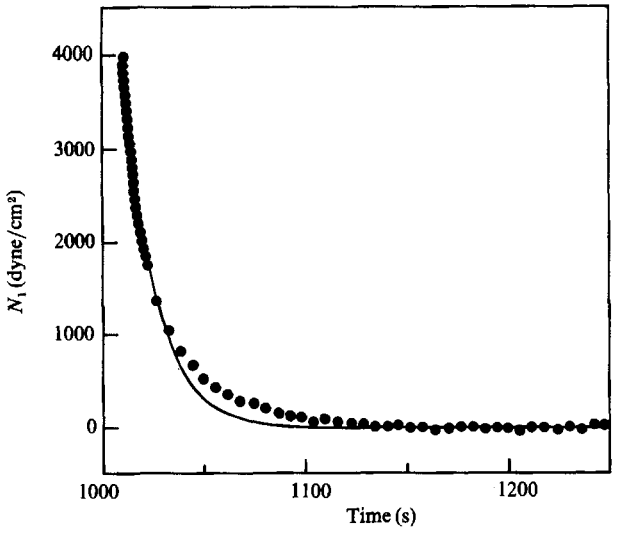


FIGURE 7. Relaxation of first normal-stress difference $N_1$ after cessation of steady-state shearing for a Boger fluid. The line is a fit of the Oldroyd-B equation, i.e. a single exponential decay.

### 5.2. *Taylor–Couette flow*

The behaviour of the test fluid in flow between concentric cylinders was examined in two different rheometers: the Rheometrics RMS-800 and the Rheometrics Stress Rheometer. In all the Taylor–Couette experiments, the Taylor number was less than $10^{-6}$, i.e. nine orders of magnitude smaller than that required for onset of the Newtonian inertial instability. On the RMS-800, a constant rotation rate was

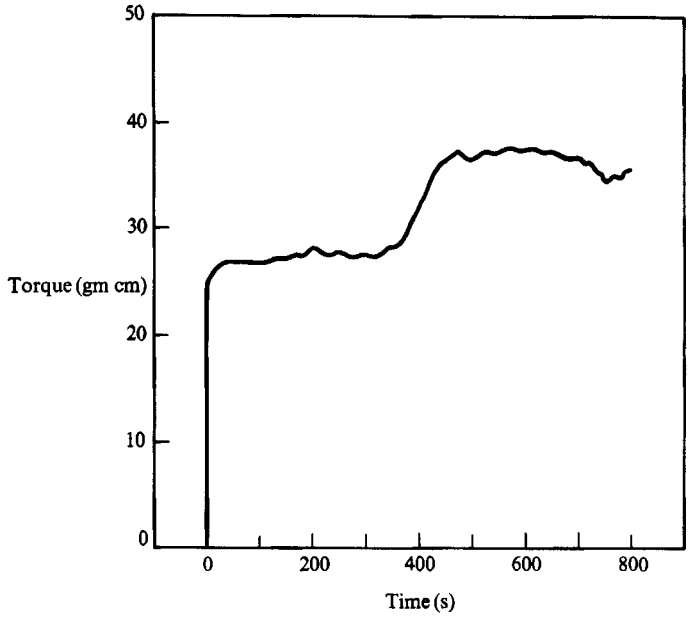


FIGURE 8. Rise in torque after start-up of steady shearing in a Taylor–Couette cell with the outer cylinder rotating and the inner cylinder fixed. Here $\epsilon = 0.0625$ and the shear rate $\dot{\gamma}$ is 2.5 $s^{-1}$.

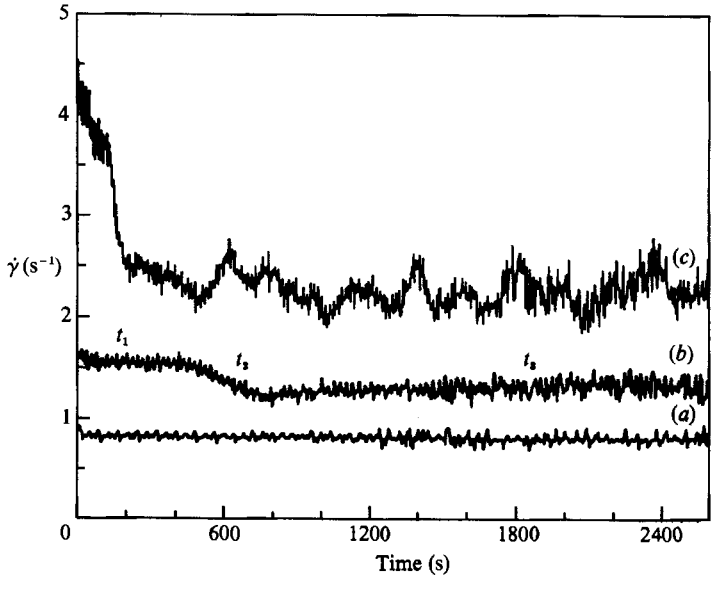


FIGURE 9. Shear rate as a function of time after start-up of shearing at constant shear stress in a Taylor–Couette cell with $\epsilon = 0.067$. The stresses imposed were 300 dyn/cm$^2$ (curve *a*); 525 dyn/cm$^2$ (curve *b*); and 625 dyn/cm$^2$ (curve *c*).

imposed on the outer cylinder and the torque on the inner cylinder was measured as a function of time. Above a critical shear rate, the torque increased dramatically after a period of time that was long compared with the longest relaxation time for the fluid. An example of this is given in figure 8. Over a period of approximately 30 s, the torque rises to an initial plateau value, which is maintained for almost 400 s. The

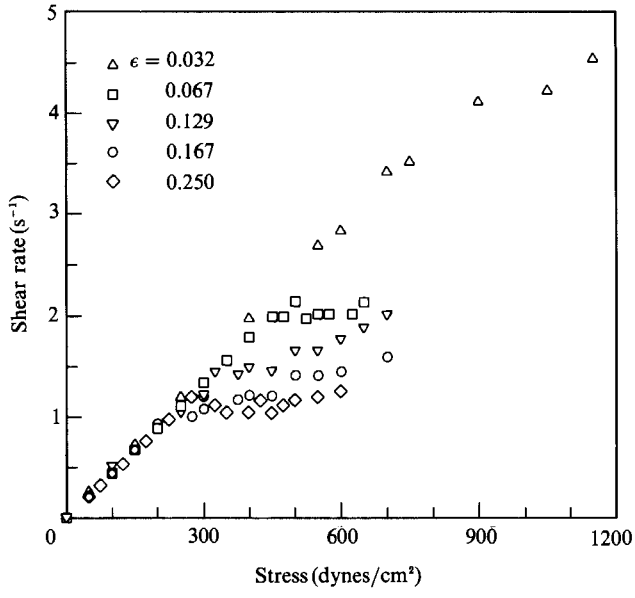


FIGURE 10. Final shear rate (after 45 min) as a function of imposed shear stress in a Taylor–Couette cell for various gap ratios.

initial plateau value is consistent with the shear stress expected in steady shear flow based on the (measured) constant viscosity $\eta = 228$ P. After 400 s, the torque on the inner cylinder increases over a period of about 100 s to a second plateau value that is about 50% higher than the first. The gradual decrease in torque after 600 s is associated with irreversible shear degradation of the fluid sample. However, if the experiment is stopped before any significant decrease in torque occurs, the results can be reproduced with the same sample. That is, the time-dependent transition associated with the jump in the torque on the inner cylinder does not result in any irreversible changes to the fluid.

The Rheometrics Stress Rheometer (RSR-8600) was used to study the onset of the transition in an attempt to avoid the prolonged high shear rates and subsequent degradation problems encountered with the RMS-800. The RSR-8600 imposes a constant stress on the inner cylinder and then measures the strain rate response. Sample results from the RSR-8600 are shown in figure 9. From these measurements, a new feature of the transition behaviour becomes apparent. When a constant stress just above the critical stress is imposed, the final shear rate after the transition is fairly constant (figure 9*b*); however, when the imposed stress is significantly above the critical value, the shear rate after the transition oscillates in time (figure 9*c*).

To determine the dependence of the onset of the transition on the dimensionless gap between the cylinders, $\epsilon \equiv d/r_i$, a set of interchangeable inner and outer cylinders was constructed. The inner cylinders were 35.0 mm in length and had radii of 14.0, 15.0, and 15.5 mm. The outer cylinders had radii of 16.0 and 17.5 mm. Data from this series of experiments are plotted in figure 10. The final shear rate after applying a constant stress for 45 min is plotted as a function of the applied stress for four different dimensionless gaps. The critical shear rate for the onset of the transition is clearly a function of the gap size. Note that since all the inner cylinders are the same length, finite-length effects will be more pronounced in the large-gap experiments.

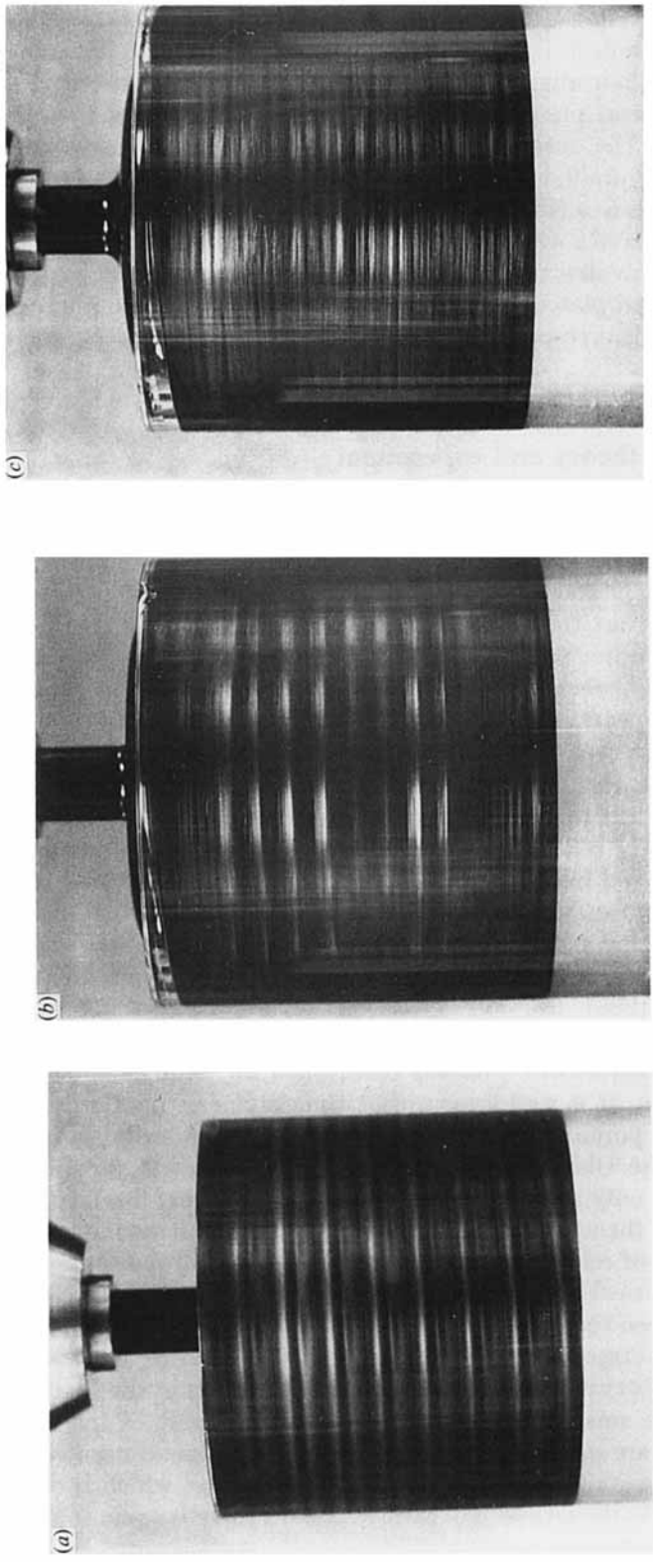


FIGURE 11. Flow visualizations in a Taylor–Couette cell. (*a*) Newtonian fluid at high Taylor number ($Ta = 3800$); (*b*) Boger fluid at negligible Taylor number ($Ta = 9.6 \times 10^{-8}$) shortly after the onset of secondary flow ($t_2$ in figure 9); (*c*) Boger fluid at negligible Taylor number after full development of secondary flow ($t_3$ in figure 9).

Flow visualization experiments were performed to determine the nature of the flow at the transition. Mica flakes about 60 μm in length were suspended in the fluid; these plate-like particles reflect light in a manner that is highly dependent on their orientation so that their alignment by the flow results in variations in the reflected light intensity. Typical photographs of the flow generated by the RSR-8600 are shown in figure 11. The onset of the transition (i.e. the time corresponding to the point marked $t_2$ in figure 9) clearly coincides with the formation of toroidal vortices similar to Taylor cells in a Newtonian fluid (figures 11*a* and 11*b*); the elastic vortices are less regular but have a wavelength comparable to the inertial vortices. However, the elastic vortices evolve (figure 11*c*) into much shorter cells as the shear rate approaches the second plateau value (point $t_3$ in figure 9). These photographs prove that the time-dependent response of these fluids in mechanical experiments is caused by a flow instability.

## 6. Comparison of theory and experiment

The theory presented in §4 qualitatively agrees with our experimental results because it predicts both the onset of an instability at vanishing Taylor number, and that the critical Deborah number for the transition should vary inversely with the gap. The non-inertial character of the instability considered here is further confirmed by our observation that the transition occurred when the inner cylinder was held stationary with the outer one rotating (see figure 8), as well as with only the inner cylinder rotating. (This is consistent with the analysis, in which the square of the quantity $\Omega_1 - \Omega_2$ appears; see (2.14) and (2.17).) Inertial effects do not lead to an instability when only the outer cylinder is rotating.

Table 2 compares the theoretical and measured critical Deborah numbers at various gap ratios. The two experimental values of $De_c$ reported in table 2 correspond to the two values of the relaxation time $\lambda$ obtained from steady-state normal stresses (lower value of $De_c$) and from relaxation of normal stresses after cessation of steady shear (higher value of $De_c$), as discussed in §5. The value of $De_c$ based on the transient measurements is in good agreement with the theoretical value; that based on steady-state measurements differs from the theoretical prediction by a factor of about two. Magda & Larson (1988) also found for the cone-and-plate and plate-and-plate instabilities (discussed in §7) that $De_c$ based on transient viscoelastic measurements was in much better agreement with the theoretical $De_c$ than that based on steady-state normal stresses. It is well known that the polymeric fluid studied here – and virtually all other polymeric fluids as well – have a distribution of molecular relaxation times. The Oldroyd-B constitutive equation, with its single relaxation time, is thus at best only a simple approximation to the real fluid. In the future we hope to develop the theory using a more accurate constitutive model that contains a realistic spectrum of relaxation times instead of the Oldroyd-B model.

Despite the theoretical limitations caused by the multiplicity of relaxation times, the agreement between theory and experiment is rather good, if the Deborah number based on transient normal stresses is used. With this measure of Deborah number, the largest variance between theory and experiment occurs at the smallest gap ratio, where effects from a small, but presumably non-zero value of the second normal stress coefficient $\Psi_2$ are most likely to be appreciable. A small negative value of $\Psi_2$ would be expected to stabilize the flow at small gap ratios, which is consistent with the trend in table 2. At the largest gap ratio in table 2 there is again some discrepancy

| Gap ratio, $\epsilon$ | $De_c$ (experimental) | | $De_c$ (theoretical) |
|---|---|---|---|
| 0.03 | 33 | 68 | 43 |
| 0.067 | 16 | 32 | 30 |
| 0.129 | 9.8 | 20 | 22 |
| 0.14 | 9.8 | 20 | 21 |
| 0.167 | 9.4 | 19 | 19 |
| 0.25 | 9.4 | 19 | 16 |

TABLE 2. Comparison of experimental and theoretical critical Deborah numbers

between theory and experiment, possibly because of stabilizing second-order terms in the gap ratio which become important when $\epsilon$ is no longer small.

Besides comparing our prediction of the critical Deborah number as a function of gap ratio, we also wish to compare the predicted wavenumber and frequency of the unstable mode with the observed values. The critical wavenumber is predicted to be $\alpha_c = 6.7$ – more than twice the critical wavenumber of the inertial instability in Newtonian fluids. It is also important to note, however, that the theory predicts a very shallow minimum in the plot of critical Deborah number versus $\alpha$ (figure 2). Thus, above the critical condition we might expect many wavenumbers to become unstable, and a complex multiple-wavelength pattern to emerge. Figure 11 (*b*, *c*) does show a complex multiple-wavelength pattern emerging in the viscoelastic instability. The average cell spacing early in time after onset of the instability seems to be comparable with that of the inertial instability in the Newtonian fluid, figure 11 (*a*), but eventually evolves to a much finer structure, with cells no more than half as tall as the Newtonian inertial cells. Thus, the wavenumber that evolves at long times (i.e. $\alpha > 6$) is consistent with the wavenumber predicted by the linear theory. The instability is predicted to have oscillatory character, a prediction consistent with the undamped oscillations present in the torque after the onset of the instability; see figure 8. We plan in the future to confirm the oscillatory nature of the instability by measuring time-dependent velocities with laser-Doppler velocimetry. In this discussion we merely note that the viscoelastic relaxation time that governs the evolution of the viscoelastic instability is long compared to typical inertial timescales that govern the evolution of the inertial instability. Thus, the long time required for development of the final cellular pattern in the viscoelastic flow as compared to the inertial Newtonian flow is not surprising.

## 7. Mechanism of instability

The mechanism of the instability can most easily be understood by referring to the dumbbell model from which the Oldroyd-B constitutive equation can be derived. The unstable eigenmode involves a radial extensional flow $\partial v_r/\partial r$ that stretches the dumbbell in the $r$-direction; see figure 12. In any time-dependent extensional flow, the maximum dumbbell stretch lags the maximum velocity gradient because of the finite relaxation time $\lambda$ of the dumbbell. The radial normal stress $\tau_{rr}$ reflects this increased radial stretch of the dumbbell and satisfies

$$\tau_{rr} + \lambda \frac{\partial}{\partial t} \tau_{rr} = 2\eta_p \frac{\partial v_r}{\partial r}. \tag{7.1}$$

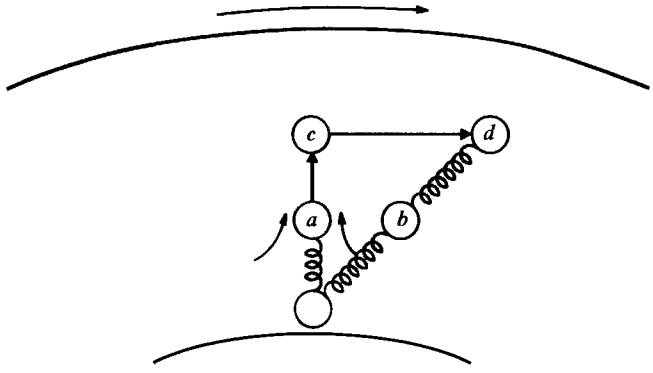


FIGURE 12. With no secondary flow, the base flow deflects a bead of an elastic dumbbell from $a$ to $b$. With a secondary radial flow, the dumbbell is stretched in the radial direction, and the base flow then deflects the bead farther; i.e. from $c$ to $d$.

Assuming small axisymmetric perturbations and using the stress and velocity representation in (2.13), we find

$$\widehat{RR} = 2\eta_p D^{-1} U', \tag{7.2}$$

where the prime denotes differentiation with respect to $r$. The additional stretching of the dumbbell in the $r$-direction produced by the perturbation radial flow increases the difference between the azimuthal ($\theta$) velocities of the two beads due to the base shearing flow. Thus the perturbation radial flow couples to the base shearing flow to produce an increased stretch of the dumbbell in the $\theta$-direction; see figure 12. This results in an increased $\theta\theta$ component of the stress tensor:

$$\left(1+\lambda\frac{\partial}{\partial t}\right)^2 \widehat{\Theta\Theta} = 2\lambda^2\dot{\gamma}^2\widehat{RR}, \tag{7.3}$$

where $\dot{\gamma}$ is the base shear rate, $\dot{\gamma} = (\Omega_2 - \Omega_1)/\epsilon$. Equation (7.3) has been obtained by neglecting all terms other than the crucial coupling term. The full expression for $\widehat{\Theta\Theta}$ is given in (A 3). Equations (7.2) and (7.3) give (note that $De = \lambda\dot{\gamma}$)

$$\widehat{\Theta\Theta} = 4\eta_p De^2 D^{-3} U'. \tag{7.4}$$

This $\theta\theta$ normal stress enters into the radial momentum balance because the streamlines are curvilinear. For simplicity we again neglect all non-essential terms and consider only the case $\eta_s \gg \eta_p$ ($S \gg 1$):

$$\frac{\partial p}{\partial r} = -\frac{\widehat{\Theta\Theta}}{r} + \eta_s \nabla^2 U. \tag{7.5}$$

The pressure also appears in the axial momentum balance equation, which for $\eta_s \gg \eta_p$ becomes

$$\frac{\partial p}{\partial z} = \eta_s \nabla^2 v_z. \tag{7.6}$$

Using (2.13), the continuity equation $v_z = i\sigma U'$, and the small-gap approximation, this becomes

$$p = -\eta_s\left(\frac{1}{\sigma^2}U''' + U'\right). \tag{7.7}$$

With this result, the pressure can be eliminated from (7.5) to give

$$U'''' - 2\sigma^2 U'' + \sigma^4 U = -4\frac{\eta_p}{\eta_s}\sigma^2 De^2 D^{-3} U'. \tag{7.8}$$

Changing to gap variables using $r \equiv r_1 + \epsilon x$, $\alpha \equiv \sigma d$, and letting the prime denote differentiation with respect to $x$ gives

$$U'''' - 2\alpha^2 U'' + \alpha^4 U = -\frac{4De^2 \epsilon D^{-3}}{S\alpha} U', \tag{7.9}$$

where $S = \eta_s/\eta_p$. Equation (7.9) bears an obvious resemblance to (3.1). The solution of (7.9) together with the boundary conditions is an overstable mode and the critical condition is given by $|De|\,\epsilon^{\frac{1}{2}}/S^{\frac{1}{2}} = 3.67$. This differs by 15% from the correct value ($|De|\,\epsilon^{\frac{1}{2}}/S^{\frac{1}{2}} = 3.19$), owing to terms we have neglected in this simplified argument.

This argument shows that the mechanism of the instability involves a coupling of a perturbation radial extensional flow to the base shearing flow. This coupling produces an azimuthal normal stress that can drive radial flow, because of curvature of the streamlines. The flow driven by the azimuthal normal stress is out of phase with the initial disturbance (via the $D^{-3}$ term in (7.9)). At sufficiently high Deborah number the flow driven by the normal stress can be stronger than the initial disturbance, and an out-of-phase response to an initially small disturbance overcompensates that disturbance and produces a growing oscillatory response.

A purely elastic instability apparently also occurs by a similar mechanism in other rotational shearing flows, namely concentric plate-and-plate flow and concentric cone-and-plate flow. These flows were used to measure the viscoelastic properties of the Boger fluid considered here, as discussed in §5. In steady shearing between a cone and plate, Magda & Larson (1988) observed a time-dependence of the material properties of these fluids above a critical shear rate, analogous to the behaviour reported here for Taylor–Couette flow. The dependence of the critical shear rate on both Deborah number and cone angle was found to be consistent with a viscoelastic instability prediced by Phan-Thien (1983, 1985) for Oldroyd-B fluids in cone-and-plate and plate-and-plate flows. This time-dependent behaviour was reproduced in the cone-and-plate geometry for the fluid used in the present study; it occurred at shear rates above those for which data were reported in §5.

The mechanism of the viscoelastic Taylor–Couette instability also bears some similarity to that which produces rod climbing, or the Weissenberg effect (Weissenberg 1947). The Weissenberg effect is observed when fluid climbs a rod rotating in a beaker of viscoelastic fluid. As in the viscoelastic Taylor–Couette and cone-and-plate and plate-and-plate instabilities, rod climbing and the secondary flow that occurs during rod climbing are driven by hoop stresses – that is, by the first normal stress difference – and are suppressed by negative values of the second normal stress difference. The similarities among mechanisms that cause the cone-and-plate, plate-and-plate, and Taylor–Couette instabilities, and the rod-climbing phenomenon, suggest that instabilities or secondary flows might occur in many rotational shearing flows of highly elastic fluids.

## Appendix A. Derivation of stability equations

To encompass previous work on viscoelastic Taylor–Couette flow (see §1), for future reference we would like our constitutive equation to contain the general

equation of the *second-order-fluid* as a special case. To allow for this, we here add a second polymer contribution to the stress,

$$\boldsymbol{\tau} = \boldsymbol{\tau}^{s} + \boldsymbol{\tau}^{p} + \boldsymbol{\tau}^{p2}; \quad \text{with} \quad \boldsymbol{\tau}^{p2} \equiv 4\Psi_2 \boldsymbol{D}\cdot\boldsymbol{D}. \tag{A 1}$$

Here $\Psi_2$ is the second normal stress coefficient, and, as discussed in §1, it can have a strong influence on the stability of Taylor–Couette flow. The constitutive equation of the second-order fluid is now recovered from (2.1) if one solves (2.4) explicitly for $\boldsymbol{\tau}^{p}$ by linearizing with respect to $\lambda$:

$$\boldsymbol{\tau}^{p} \approx 2(\eta_s + \eta_p)\boldsymbol{D} - 2\eta_p \lambda \overset{\nabla}{\boldsymbol{D}}.$$

The first normal stress coefficient, $\Psi_1$, equals $2\eta_p\lambda$. Although in the body of the paper, $\boldsymbol{\tau}^{p2}$ was not included (that is, $\Psi_2$ was set to zero), for future consideration we retain $\boldsymbol{\tau}^{p2}$ in the general development of the stability equations.

When the expressions for the perturbed velocity components in (2.13*a*) are substituted into the continuity equation (2.9), we find

$$\frac{1}{r}(rU)' + \mathrm{i}\sigma W = 0, \tag{A 2}$$

where the prime denotes differentiation with respect to $r$.

Substituting the stress and velocity components in (2.13) into (2.4), we can solve for the $r$-dependent stress functions:

$$\left.\begin{aligned}
&\frac{\widehat{ZZ}}{\eta_p} = 2\mathrm{i}\sigma W \boldsymbol{D}^{-1}; \quad \frac{\widehat{RR}}{\eta_p} = 2U'\boldsymbol{D}^{-1}; \quad \frac{\widehat{RZ}}{\eta_p} = (\mathrm{i}\sigma U + W')\boldsymbol{D}^{-1},\\
&\frac{\widehat{R\Theta}}{\eta_p} = \left[r\left(\frac{V}{r}\right)' - \lambda B r^{-2}\left(6\frac{U}{r} + 2U'\right) - 4\lambda B r^{-2} U' \boldsymbol{D}^{-1}\right]\boldsymbol{D}^{-1},\\
&\frac{\widehat{\Theta Z}}{\eta_p} = [\mathrm{i}\sigma V - 2\lambda B r^{-2}(\mathrm{i}\sigma U + W')\boldsymbol{D}^{-1} - 2\lambda B r^{-2} W']\boldsymbol{D}^{-1},\\
&\frac{\widehat{\Theta\Theta}}{\eta_p} = 2\frac{U}{r}\boldsymbol{D}^{-1} + 48\lambda^2 U B^2 r^{-5}\boldsymbol{D}^{-1} + 24\lambda^2 U B^2 r^{-5}\boldsymbol{D}^{-2}\\
&\qquad + 8\lambda^2 U' B^2 r^{-4}\boldsymbol{D}^{-2}(1 + 2\boldsymbol{D}^{-1}) - 4\lambda r\left(\frac{V}{r}\right)' B r^{-2}\boldsymbol{D}^{-1}(1 + \boldsymbol{D}^{-1}).
\end{aligned}\right\} \tag{A 3}$$

In the above

$$\boldsymbol{D} \equiv 1 - \mathrm{i}\omega\lambda.$$

### A.1. *Linear stability equations*

We now substitute (A 1) into the momentum balance equations (2.6)–(2.8), with the stress and velocity components given by (2.13) and (A 3), and use (A 2) to eliminate $W(r)$:

$$\begin{aligned}
&\left\{\left(\frac{1}{r}(rU)'\right)' + (\mathrm{i}\sigma)^2 U\right\}[\eta_p \boldsymbol{D}^{-1} + \eta_s] - 24\eta_p \lambda^2 U B^2 r^{-6}\boldsymbol{D}^{-1}(2 + D^{-1})\\
&\quad - 8\eta_p \lambda^2 U' B^2 r^{-5}\boldsymbol{D}^{-2}(1 + 2\boldsymbol{D}^{-1}) + 4\eta_p \lambda\left(\frac{V}{r}\right)' B r^{-2}\boldsymbol{D}^{-1}(1 + \boldsymbol{D}^{-1})\\
&\quad + \Psi_2 B\left[-4r^{-1}\left(\frac{V}{r}\right)'' + 4r^{-2}\left(\frac{V}{r}\right)' - 2(\mathrm{i}\sigma)^2 r^{-2} V\right]\\
&= \frac{\partial p}{\partial r} - \mathrm{i}\omega U\rho - \frac{2(Ar + Br^{-1})V}{r}\rho,
\end{aligned} \tag{A 4a}$$

$$\left\{\left(\frac{1}{r}(rV)'\right)'+(\mathrm{i}\sigma)^2V\right\}[\eta_p D^{-1}+\eta_s]-\lambda r^{-2}\left[\left(B\left(\frac{6U}{r}+2U'\right)\right)'-2B\left(\frac{1}{r}(rU)'\right)'\right]D^{-1}\eta_p$$
$$-\lambda r^{-2}[4(BU')'-2B\left(\frac{1}{r}(rU)'\right)']D^{-2}\eta_p-2\lambda(\mathrm{i}\sigma)^2Br^{-2}UD^{-2}\eta_p$$
$$+\Psi_2 B\left[-4r^{-2}\left(U'+\frac{U}{r}\right)'-2(\mathrm{i}\sigma)^2r^{-2}U+2r^{-2}\left(\frac{1}{r}(rU)'\right)'\right]$$
$$=-\mathrm{i}\omega V\rho+2CU\rho, \tag{A 4b}$$

$$\left\{\frac{1}{\sigma^2}\frac{1}{r}\left[r\left(\frac{1}{r}(rU)'\right)'\right]'-\frac{1}{r}(rU)'\right\}[\eta_p D^{-1}+\eta_s]-2\Psi_2 B\frac{1}{r}\left(\frac{V}{r}\right)'=p-\frac{\mathrm{i}\omega}{\sigma^2}\frac{1}{r}(rU)'\rho. \tag{A 4c}$$

The pressure $p$ can be eliminated between (A 4*a*) and (A 4*c*) giving

$$\left[\frac{1}{\sigma^2}\left[\frac{1}{r}\left(r\left[\frac{1}{r}(rU)'\right]'\right)'\right]'-2\left[\frac{1}{r}(rU)'\right]'-(\mathrm{i}\sigma)^2U\right][\eta_p D^{-1}+\eta_s]+24\eta_p\lambda^2UB^2r^{-6}D^{-1}(2+D^{-1})$$
$$+8\eta_p\lambda^2U'B^2r^{-5}D^{-2}(1+2D^{-1})-4\eta_p\lambda\left(\frac{V}{r}\right)'Br^{-2}D^{-1}(1+D^{-1})$$
$$-\Psi_2 B\left[-4r^{-1}\left(\frac{V}{r}\right)''+4r^{-2}\left(\frac{V}{r}\right)'-2(\mathrm{i}\sigma)^2r^{-2}V-2\left[\frac{1}{r}\left(\frac{V}{r}\right)'\right]'\right]$$
$$=\mathrm{i}\omega U\rho+2(A+Br^{-2})V\rho-\frac{\mathrm{i}\omega}{\sigma^2}\left[\frac{1}{r}(rU)'\right]'\rho. \tag{A 5}$$

The boundary conditions obtained from (2.9) are

$$V=U=U'=0 \quad \text{at} \quad r=r_1 \quad \text{and} \quad r_2. \tag{A 6}$$

The boundary condition $U'=0$ was obtained from the condition $W=0$ and the continuity equation (A 1).

A.1.1. *Dimensionless groups*

We cast the above equations into dimensionless form by setting $R=r/r_1$ and defining the following dimensionless groups:

$$\left.\begin{aligned} De\equiv\frac{2B\lambda}{r_1^2};\quad \psi\equiv\frac{\Psi_2}{\lambda\eta_p};\quad S\equiv\frac{\eta_s}{\eta_p},\\ \epsilon\equiv\frac{d}{r_1};\quad \alpha\equiv\sigma d,\\ Re\equiv\frac{\Omega_1 r_1 d\rho}{\eta_p+\eta_s};\quad \beta\equiv\frac{\Omega_2}{\Omega_1}-1. \end{aligned}\right\} \tag{A 7}$$

There are two dimensionless frequencies in our problem. One, $\omega\lambda$, is scaled on the viscoelastic relaxation time. The other, $(\omega/\Omega_1)Re$, is scaled on an inertial timescale. Since both negligible inertia and negligible viscoelasticity are important limits of our equations, in this Appendix we shall avoid choosing a dimensionless frequency and leave a dimensional $\omega$ in the equations. The two limits are then achieved simply by setting $\lambda$ and $De$ to zero or $Re$ to zero.

In what follows, it will be convenient to use the following groupings of parameters:

$$\tilde{A}\equiv\frac{A\epsilon}{\Omega_1}=\frac{\epsilon[(1+\epsilon)^2(\beta+1)-1]}{(1+\epsilon)^2-1};\quad \tilde{B}\equiv\frac{B\epsilon}{\Omega_1 r_1^2}=-\frac{\beta\epsilon(1+\epsilon)^2}{(1+\epsilon)^2-1}. \tag{A 8}$$

A.1.2. *Dimensionless equations*

With these definitions (A 4*b*) takes the following dimensionless form:

$$V''+\frac{V'}{R}-\left[\frac{\alpha^2}{\epsilon^2}+\frac{1}{R^2}-\frac{i\omega Re\,(1+S)}{\Omega_1\,\epsilon(D^{-1}+S)}\right]V=\frac{1}{R^2}\left[K_1\,U''+K_2\frac{U'}{R}+K_3\frac{U}{R^2}\right], \tag{A 9}$$

where

$$K_1\equiv De\left[\frac{D^{-2}+\psi}{D^{-1}+S}\right],\quad K_2\equiv De\left[\frac{D^{-1}(2-D^{-1})+\psi}{D^{-1}+S}\right], \tag{A 10$a$, $b$}$$

$$K_3\equiv\frac{-De\,[D^{-1}(2-D^{-1})+\psi]}{D^{-1}+S}-\frac{\alpha^2R^2\,De\,(\psi+D^{-2})}{\epsilon^2(D^{-1}+S)}+\frac{2Re\,\tilde{A}(1+S)}{\epsilon^2(D^{-1}+S)}R^4. \tag{A 10$c$}$$

Equation (A 5) takes the form

$$U''''+\frac{2}{R}U'''-\left(\frac{3}{R^2}+2\frac{\alpha^2}{\epsilon^2}-\frac{i\omega Re\,(1+S)}{\Omega_1\,\epsilon(D^{-1}+S)}\right)U''+E_2\,U'+F_2\,U+G_2\,V''+H_2\,V'+I_2\,V=0, \tag{A 11}$$

with

$$\left.\begin{aligned}
E_2&=\left(\frac{3}{R^3}-\frac{2\alpha^2}{\epsilon^2R}\right)+\frac{2De^2\,\alpha^2\,D^{-2}(1+2D^{-1})}{\epsilon^2R^5}\frac{}{D^{-1}+S}+\frac{1}{R}\frac{i\omega Re\,(1+S)}{\Omega_1\,\epsilon(D^{-1}+S)},\\
F_2&\equiv\frac{\alpha^4}{\epsilon^4}+\frac{2\alpha^2}{\epsilon^2R^2}-\frac{3}{R^4}+\frac{6De^2\,\alpha^2\,D^{-2}(1+2D)}{\epsilon^2R^6}\frac{}{D^{-1}+S}-\frac{1}{R^2}\frac{i\omega Re\,(1+S)}{\Omega_1(D^{-1}+S)\,\epsilon}-\frac{i\omega Re\,\alpha^2(1+S)}{\Omega_1\,\epsilon^3(D^{-1}+S)},\\
G_2&\equiv\frac{\alpha^2\psi\,De}{\epsilon^2R^2(D^{-1}+S)},\quad H_2\equiv\frac{-3\alpha^2\psi\,De}{\epsilon^2R^3(D^{-1}+S)}-\frac{2\alpha^2\,De\,D^{-1}(1+D^{-1})}{\epsilon^2R^3(D^{-1}+S)},\\
I_2&\equiv\frac{\alpha^2\psi\,De}{\epsilon^2R^2(D^{-1}+S)}\left(\frac{1}{R^2}-\frac{\alpha^2}{\epsilon^2}\right)+\frac{2\alpha^2\,De\,D^{-1}(1+D^{-1})}{\epsilon^2R^4(D^{-1}+S)}-\frac{2\alpha^2\,Re\,(1+S)}{\epsilon^4(D^{-1}+S)}\left[\tilde{A}+\frac{\tilde{B}}{R^2}\right].
\end{aligned}\right\} \tag{A 12}$$

A.2. *Small-gap equations*

In a later paper, the solution to the above set of equations for arbitrary gap ratio $\epsilon$ will be sought. Here we content ourselves with the limiting forms of (A 9)–(A 12) when $\epsilon$ is small. To obtain the small-gap limit, we express $R$ as $1+\epsilon x$ where $x$ runs from 0 to 1, and then neglect any term multiplied by $\epsilon$ unless that term is also multiplied by a possibly large parameter, namely $De$ or $Re$. Doing this, we get (the prime now denotes differentiation with respect to $x$)

$$V''-\left[\alpha^2-\frac{i\omega Re\,\epsilon(1+S)}{\Omega_1(D^{-1}+S)}\right]V=K_1\,U''+K_2\,\epsilon U'-\left(\alpha^2K_1-\frac{2Re\,\tilde{A}(1+S)}{D^{-1}+S}\right)U \tag{A 13}$$

and

$$U''''-\left[2\alpha^2-\frac{i\omega Re\,\epsilon(1+S)}{\Omega_1(D^{-1}+S)}\right]U''+\hat{E}_2\,U'+\hat{F}_2\,U+\hat{G}_2\,V''+\hat{H}_2\,V'+\hat{I}_2\,V=0, \tag{A 14}$$

where now

$$K_1\equiv De\left[\frac{D^{-2}+\psi}{D^{-1}+S}\right],\quad K_2\equiv De\left[\frac{D^{-1}(2-D^{-1})+\psi}{D^{-1}+S}\right], \tag{A 15$a$, $b$}$$

$$\hat{E}_2\equiv 2De^2\,\epsilon\alpha^2\frac{D^{-2}(1+2D^{-1})}{D^{-1}+S}+\frac{i\omega Re\,\epsilon^2(1+S)}{\Omega_1(D^{-1}+S)}, \tag{A 15$c$}$$

$$\hat{F}_2 \equiv \alpha^4 + 6De^2\epsilon^2\alpha^2\frac{D^{-2}(1+2D^{-1})}{D^{-1}+S} - \frac{i\omega Re\,\epsilon(1+S)}{Q_1(D^{-1}+S)}(\epsilon^2+\alpha^2), \tag{A 15d}$$

$$\hat{G}_2 \equiv \frac{\alpha^2\psi De}{D^{-1}+S}, \quad \hat{H}_2 \equiv \frac{-3\psi De\,\epsilon\alpha^2}{D^{-1}+S} - \frac{2De\,\epsilon\alpha^2 D^{-1}(1+D^{-1})}{D^{-1}+S} \tag{A 15e,f}$$

$$\hat{I}_2 \equiv \frac{\psi De\,\alpha^2}{D^{-1}+S}(\epsilon^2-\alpha^2) + \frac{2De\,\epsilon^2\alpha^2 D^{-1}(1+D^{-1})}{D^{-1}+S} - \frac{2Re\,\alpha^2\epsilon(1+S)}{D^{-1}+S}(1+\beta x). \tag{A 15g}$$

For the Oldroyd-B equation ($\psi = 0$) without inertia ($Re = 0$), noticing that the $U'$ term in (A 13) can be dropped since it is higher order in $\epsilon$ than the $U''$ term, (A 13) reduces simply to

$$V'' - \alpha^2 V = K_1(U'' - \alpha^2 U). \tag{A 16}$$

In the light of the boundary conditions (A 6), this implies that

$$V = K_1 U. \tag{A 17}$$

This important simplification allows us to eliminate $V$ in (A 14) (with $\psi$ and inertial terms dropped):

$$U'''' - 2\alpha^2 U'' + \alpha^4 U + De^2\epsilon\alpha^2\tilde{c}U' = 0, \tag{A 18}$$

with

$$\tilde{c} \equiv 2\left[\frac{D^{-2}(1+2D^{-1})(D^{-1}+S) - D^{-3}(1+D^{-1})}{(D^{-1}+S)^2}\right]. \tag{A 19}$$

## Appendix B. Approximate Galerkin solution technique

The eigenvalue problem to be solved is (equation (3.1)):

$$U'''' - 2\alpha^2 U'' + \alpha^4 U + \alpha^3 \Lambda U' = 0, \tag{B 1a}$$

together with the boundary conditions

$$U = U' = 0; \quad x = \pm\tfrac{1}{2}. \tag{B 1b}$$

In (B 1*b*) we have shifted the coordinates relative to those used in (2.18). Our aim is to find approximate eigensolutions for the problem defined by (B 1) (if they exist). These can be used to deduce approximate conditions for hydrodynamic instability, and can be used as initial guesses in the more accurate shooting method discussed in §3.2.

Following Chandrasekhar, we expand $U$ in a suitably normalized set of complete basis functions on the interval $-\frac{1}{2} \leqslant x \leqslant \frac{1}{2}$. We choose the functions that are defined and discussed by Grosch & Salwen (1968) in their study of Poiseuille flow and are the solutions of the following eigenvalue problem:

$$\phi^{iv} - 2\alpha^2\phi'' + \alpha^4\phi = \beta^4\phi, \tag{B 2a}$$

$$\phi = \phi' = 0; \quad x = \pm\tfrac{1}{2}. \tag{B 2b}$$

The two sets of complete functions that satisfy this eigenvalue problem are found in Grosch & Salwen (1968). We shall denote these two function sets $\phi_n^1$ and $\phi_n^2$, with '1' denoting the even set and '2' denoting the odd, and their respective eigenvalues $\beta_n^1$ and $\beta_n^2$. They have been chosen such that they are completely orthonormal, i.e.

$$\langle\phi_n^1, \phi_m^1\rangle = \delta_{nm}, \quad \langle\phi_n^2, \phi_m^2\rangle = \delta_{nm}, \quad \langle\phi_n^1, \phi_m^2\rangle = 0, \tag{B 3a, b, c}$$

where the inner products in (B 3) are defined by the relation

$$\langle \cdot, \cdot \rangle \equiv \int_{-\frac{1}{2}}^{\frac{1}{2}} \cdot \cdot \, \mathrm{d}x. \tag{B4}$$

Since they are complete, we can now expand $U$ in these functions, viz.

$$U = \sum_{n=1}^{\infty} [a_n \phi_n^1 + b_n \phi_n^2]. \tag{B 5}$$

The eigenvalue condition can now be determined by first substituting this expansion into (B 1) and taking inner products with both $\phi_n^1$ and $\phi_n^2$ to obtain the two conditions

$$\sum_{n=1}^{\infty} [\alpha^3 \Lambda b_n \langle \phi_n^{2'}, \phi_m^1 \rangle + a_n (\beta_n^1)^4 \delta_{nm}] = 0, \tag{B 6a}$$

$$\sum_{n=1}^{\infty} [\alpha^3 \Lambda a_n \langle \phi_n^{1'}, \phi_m^2 \rangle + b_n (\beta_n^2)^4 \delta_{nm}] = 0. \tag{B 6b}$$

In deriving (B 6), we have used the facts that

$$\langle \phi_n^{1'}, \phi_m^1 \rangle = \langle \phi_n^{2'}, \phi_m^2 \rangle = 0,$$

since the derivative inverts the parity of the basis functions. To determine the eigenvalues $\Lambda$ we solve (B 6$a$) for the $a_n$ in terms of the $b_n$ and then, substituting this result into (B 6$b$), we obtain the infinite matrix condition

$$\sum_{j=1}^{\infty} \left\{ \sum_{n=1}^{\infty} \left[ \frac{\alpha^6 \Lambda^2}{(\beta_n^1)^4} \langle \phi_m^2, \phi_n^{1'} \rangle \langle \phi_n^1, \phi_j^{2'} \rangle \right] - (\beta_j^2)^4 \delta_{mj} \right] b_j = 0. \tag{B 7}$$

For a non-trivial solution to exist, the eigenvalues $\Lambda_n$ must satisfy the condition

$$\left| \sum_{n=1}^{\infty} \left[ \frac{\alpha^6 \Lambda^2}{(\beta_n^1)^4} \langle \phi_m^2, \phi_n^{1'} \rangle \langle \phi_n^1, \phi_j^{2'} \rangle \right] - (\beta_j^2)^4 \delta_{mj} \right| = 0. \tag{B 8}$$

Once the inner products in (B 8) are calculated, this condition becomes an infinite polynomial for the infinite discrete eigenvalues $\Lambda_n$. To obtain analytic approximations to these eigenvalues we make an approximation which has been useful in other contexts and neglect the non-diagonal elements in the inner-product matrices, i.e.

$$\langle \phi_n^{2'}, \phi_m^1 \rangle \approx \langle \phi_n^{2'}, \phi_n^1 \rangle \delta_{nm}, \quad \langle \phi_n^{1'}, \phi_m^2 \rangle \approx \langle \phi_n^{1'}, \phi_n^2 \rangle \delta_{nm}. \tag{B 9a, b}$$

We demonstrate in the text (cf. table 1) that these approximations are useful in the present context.

Substituting (B 9) into the eigenvalue condition (B 8), we obtain the following expression for the eigenvalues:

$$(\Lambda_n)^2 \approx \frac{[\beta_n^2]^4 [\beta_n^1]^4}{\alpha^6 \langle \phi_n^{2'}, \phi_n^1 \rangle \langle \phi_n^{1'}, \phi_n^2 \rangle}. \tag{B 10}$$

We note that a simple calculation shows that the second inner product in the denominator is always negative and thus (B 10) describes an infinite series of purely imaginary, conjugate eigenvalues. We show in §4 that these solutions imply flow instability. Because the eigenvalues $\beta_n^1$ and $\beta_n^2$ increase with increasing $n$, the absolute value of $\Lambda_n$ also increases. The eigenvalue of smallest magnitude is thus $\pm \Lambda_1$.

## REFERENCES


BEARD, D. W., DAVIES, M. H. & WALTERS, K. 1966 The stability of elastico-viscous flow between rotating cylinders. Part 3. Overstability in viscous and Maxwell fluids. *J. Fluid Mech.* **24**, 321–334.

BEAVERS, G. S. & JOSEPH, D. D. 1974 Tall Taylor cells in polyacrylamide solutions. *Phys. Fluids* **17**, 650–651.

BIRD, R. B., CURTISS, C. F., ARMSTRONG, R. C. & HASSAGER, O. 1987 *Dynamics of Polymeric Liquids*, vol. 2, 2nd edn. Wiley-Interscience.

BOGER, D. V. 1977/1978 A highly elastic constant-viscosity fluid. *J. Non-Newtonian Fluid Mech.* **3**, 87–91.

CHANDRASEKHAR, S. 1961 *Hydrodynamic Stability*. Clarendon.

COLEMAN, B. D. & NOLL, W. 1961 Foundations of linear viscoelasticity. *Rev. Mod. Phys.* **33**, 239–249.

COLES, D. 1965 Transition in circular Couette flow. *J. Fluid Mech.* **21**, 385–425.

CONTE, S. D. 1966 The numerical solution of linear boundary value problems. *SIAM Rev.* **8**, 309–321.

DATTA, S. K. 1964 Note on the stability of an elasticoviscous liquid in Couette flow. *Phys. Fluids* **7**, 1915–1919.

DENN, M. M. & ROISMAN, J. J. 1969 Rotational stability and measurement of normal stress functions in dilute polymer solutions. *AIChE J.* **15**, 454–459.

DRAZIN, P. G. & REID, W. H. 1981 *Hydrodynamic Stability*. Cambridge University Press.

FENSTERMACHER, P. R., SWINNEY, H. L. & GOLLUB, J. P. 1979 Dynamic instabilities and the transition to chaotic Taylor vortex flow. *J. Fluid Mech.* **94**, 103–128.

GIESEKUS, H. 1966 Zur Stabilität von Strömungen viskoelastisher Flüssigkeiten. *Rheol. Acta* **5**, 239–252.

GIESEKUS, H. 1972 On instabilities in Poiseuille and Couette flows of viscoelastic fluids. *Prog. Heat Mass Transfer* **5**, 187–193.

GINN, R. F. & DENN, M. M. 1969 Rotational stability in viscoelastic liquids. *AIChE J.* **15**, 450–454.

GOLLUB, J. P. & SWINNEY, H. L. 1975 Onset of turbulence in a rotating fluid. *Phys. Rev. Lett.* **35**, 927–930.

GREEN, J. & JONES, W. M. 1982 Couette flow of dilute solutions of macromolecules: embryo cells and overstability. *J. Fluid Mech.* **119**, 491–505.

GREENBERG, M. D. 1978 *Foundations of Applied Mathematics*. Prentice-Hall.

GROSCH, C. E. & SALWEN, H. 1968 The stability of steady and time-dependent plane Poiseuille flow. *J. Fluid Mech.* **34**, 177–205.

HAYES, J. W. & HUTTON, J. F. 1972 The effect of very dilute polymer solutions on the formation of Taylor vortices. Comparison of theory with experiment. *Prog. Heat Mass Transfer* **5**, 195–209.

JONES, W. M., DAVIES, D. M. & THOMAS, M. C. 1973 Taylor vortices and the evaluation of material constants: a critical assessment. *J. Fluid Mech.* **60**, 19–41.

KEENTOK, M., GEORGESCU, A. G., SHERWOOD, A. A. & TANNER, R. I. 1980 The measurement of the second normal stress difference for some polymer solutions. *J. Non-Newtonian Fluid Mech.* **6**, 303–324.

LOCKETT, F. J. & RIVLIN, R. S. 1968 Stability in Couette flow of a viscoelastic fluid. Part I. *J. Méc.* **7**, 475–498.

MACKAY, M. E. & BOGER, D. V. 1987 An explanation of the rheological properties of Boger fluids. *J. Non-Newtonian Fluid Mech.* **22**, 235–243.

MAGDA, J. J. & LARSON, R. G. 1988 A transition in ideal elastic liquids during shear flow. *J. Non-Newtonian Fluid Mech.* **30**, 1–19.

MAGDA, J. J., LOU, J., BAEK, S.-G. & DEVRIES, K. L. 1990 The second normal stress difference of a Boyer fluid. *Polymer* (submitted).

MILLER, C. & GODDARD, J. D. 1979 Appendix to Goddard, J. D. 1979 Polymer fluid mechanics. *Adv. Appl. Mech.* **19**, 143–219.

PHAN-THIEN 1983 Coaxial-disk flow of an Oldroyd-B fluid: exact solution and stability. *J. Non-Newtonian Fluid Mech.* **13**, 325–340.

PHAN-THIEN, N. 1985 Cone-and-plate flow of the Oldroyd-B fluid is unstable. *J. Non-Newtonian Fluid Mech.* **17**, 37–44.

PRILUTSKI, G., GUPTA, R. K., SRIDHAR, T. & RYAN, M. E. 1983 Model viscoelastic liquids. *J. Non-Newtonian Fluid Mech.* **12**, 233–241.

RAMACHANDRAN, S., GAO, H. W. & CHRISTIANSEN, E. B. 1985 Dependence of viscoelastic flow functions on molecular structure for linear and branched polymers. *Macromolecules* **18**, 695–699.

RUBIN, H. & ELATA, C. 1966 Stability of Couette flow of dilute polymer solutions. *Phys. Fluids* **9**, 1929–1933.

SHAQFEH, E. S. G. & ACRIVOS, A. 1987 The effects of inertia on the stability of the convective flow in inclined particle settlers. *Phys. Fluids* **30**, 960–973.

SHAQFEH, E. S. G., LARSON, R. G. & FREDRICKSON, G. H. 1989 The stability of gravity driven viscoelastic film-flow at low to moderate Reynolds number. *J. Non-Newtonian Fluid Mech.* **31**, 87–113.

SMITH, M. M. & RIVLIN, R. S. 1972 Stability in Couette flow of a viscoelastic fluid. Part II. *J. Méc.* **11**, 69–94.

SRIDHAR, T., GUPTA, R. K., BOGER, D. V. & BINNINGTON, R. 1986 Steady spinning of the Oldroyd fluid B. II: Experimental results. *J. Non-Newtonian Fluid Mech.* **21**, 115–126.

SUN, Z.-S. & DENN, M. M. 1972 Stability of rotational Couette flow of polymer solutions. *AIChE J.* **18**, 1010–1015.

TAYLOR, G. I. 1923 Stability of a viscous liquid contained between two rotating cylinders. *Phil. Trans. R. Soc. Lond.* A **223**, 289–343.

THOMAS, R . H. & WALTERS, K. 1964 The stability of elastico-viscous flow between rotating cylinders. Part 1. *J. Fluid Mech.* **18**, 33–43.

WEISSENBERG, K. 1947 A continuum theory of rheological phenomena. *Nature* **159**, 310–311.